Available online at www.sciencedirect.com

ScienceDirect

Solar Energy 101 (2014) 63–73

SOLAR ENERGY

www.elsevier.com/locate/solener

Three-dimensional SOlar RAdiation Model (SORAM) and its application to 3-D urban planning

Róbert Erdélyi [a], Yimin Wang [a,*], Weisi Guo [b], Edward Hanna [c], Giuseppe Colantuono [d]

[a] Solar Physics and Space Plasma Research Centre (SP2RC), School of Mathematics and Statistics, University of Sheffield, Sheffield S3 7RH, UK
[b] School of Engineering, University of Warwick, Coventry CV4 7AL, UK
[c] Department of Geography, University of Sheffield, Sheffield S10 2TN, UK
[d] The Sheffield Solar Farm, Department of Physics and Astronomy, University of Sheffield, Sheffield S3 7RH, UK

Received 17 August 2013; received in revised form 12 December 2013; accepted 17 December 2013
Available online 10 January 2014

Communicated by Associate Editor: Frank Vignola

Abstract

The aim of this work is to evaluate the potential direct and diffuse solar radiation aggregated at a point location in an urban area. With the three-dimensional (3D) SOlar RAdiation Model (SORAM) presented here, the paper makes three key contributions. Firstly, the model augments the Perez et al. (1990) model by accounting for the aggregated contribution of diffuse radiation using ray-tracing methods. Secondly, the model demonstrates the use of a randomly generated city building distribution and terrain map to simulate the 3D urban solar radiation exposure at any time or over a selected time period. Thirdly, we validate our results using empirical sunlight data measured from a real urban area (Sheffield Solar Farm), and also validate our results against the Perez et al. (1990) model under conditions of no shading.

Keywords: 3D; Shading condition; Solar radiation

1. Introduction

Solar radiation models are used to estimate how much solar irradiance can be collected at a location on the Earth's surface. Most existing models typically do not take into account the effects caused by urban shading (i.e. shadows cast by buildings, trees and other obstacles). The global radiation received on a point over a given time period is composed of direct radiation (i.e. that part which emanates directly from the Sun), diffuse radiation (the other part that is scattered by the Earth's atmosphere) and reflected radiation (reflected by obstacles surrounding the location). In most cases, the reflected radiation is negligible (HEMI, 2000) and is therefore ignored here.

1.1. Motivation

A sustainable city needs to generate a large fraction of its energy consumption using renewable energy sources. Large-scale photovoltaic (PV) solar-energy installations are seen as a potential solution for future cities (Hofierka and Kanuk, 2009). Grid-connected PV systems can aid peak shaving, minimize transmission and distribution losses and increase grid capacity since they generate electricity close to, or even at the consumers' point of use. Especially in great commercial areas, daytime peak load profiles are consistent with solar generation profiles (da Silva Jardim et al., 2008). Accurate local-scale

* Corresponding author. Address: Solar Physics and Space Plasma Research Centre (SP2RC), School of Mathematics and Statistics, University of Sheffield, F27 Hicks Building, Hounsfield Rd, Sheffield S3 7RH, UK. Tel.: +44 (0)7734803865.
E-mail address: yimin.wang@sheffield.ac.uk (Y. Wang).

0038-092X/$ - see front matter © 2013 Elsevier Ltd. All rights reserved.
http://dx.doi.org/10.1016/j.solener.2013.12.023

(e.g. city-wide) models of both the spatial and temporal distributions of solar radiation are needed. The aim of this paper is to provide a working model for estimating the total solar energy received at a point on a sloping PV cell surface, particularly those that are subject to intermittent shading from urban terrain. The model we develop is a key enabler for the efficient deployment of PV panels at both the street level and on the walls of buildings. In order for a sustainable city or householder to determine the position, size, optimised slope and azimuth angles of PV installations, this model can be implemented to display the solar radiation distribution for each point on a surface (e.g. roof, walls and ground etc.) of a city or house. Moreover, this model can solve the problem raised in Fartaria and Pereira (2013), which is how to calculate shadow losses caused by 2-axis moving PV module trackers in PV collector fields.

1.2. Review

In the literature several solar-radiation software tools and models have been established. The most widely used software tools are the ArcGIS Solar Analyst (ArcGIS, 2012), the GRASS GIS r.sun (Suri and Hofierka, 2004; Hofierka and Zlocha, 2012), the PVSYST (PVsyst 6 Help, 2013) and PV*Sol (2013). The main drawback of the ArcGIS Solar Analyst is that by using stereographic projection, the whole sky is projected as a flat circle, with inevitable geometric inaccuracies due to the spatial distortion during the translation from 3D to 2D. The description of the methodology of the GRASS GIS r.sun can be found in the article by Suri and Hofierka (2004) with further extension from 2D to 3D version in Hofierka and Zlocha (2012). GRASS GIS r.sun and PVSYST assume an isotropic sky for diffuse radiation. Although this simplification is easy to use, it is imprecise and several anisotropic sky models have been shown to be more accurate (Muneer, 2004). PV*Sol is designed for the calculation of shadows cast only by static obstacles (Fartaria and Pereira, 2013).

There are other models and algorithms used to calculate shading losses like Perpinan (2012); Navarte and Lorenzo (2008) and Lorenzo et al. (2011), which compute shadow shapes with dimensions for each position of the Sun, followed by a calculation of multiple shadows' joint effect. This method is usually complicated as the intersection of the shadows is too complex to calculate and can lead to errors when simplifications are made (Fartaria and Pereira, 2013). Similarly, Fartaria and Pereira (2013) computes shadow losses caused by 2-axis moving PV module trackers. Their paper considers the shaded fraction of the PV array area affected by the shading. This method is precise when considering only PV collector fields that are obstructed by simple regular geometric shapes, but can not adequately cope with complex or combined shapes that are found in urban areas.

In other literature, Melo et al. (2013) and Redweik et al. (2013) also estimate shadow losses at PV surfaces, but when calculating diffuse radiation by using diffuse shading factor in Melo et al. (2013) or the sky view factor in Redweik et al. (2013), they do not consider the angle of incidence of solar energy contribution from each sky segment. Under the diffuse radiation framework employed in Melo et al. (2013) and Redweik et al. (2013), provided that all the obstacle dimensions are the same, their orientation with respect to the PV cell is not important. Our work improves on this by attempting to refine the Perez et al. (1990) model, enabling it to calculate the angle of incidence for each diffuse ray.

Alternative methods, such as that adopted by Orioli and Gangi (2012), use photographs taken on site to determine the level of shadowing. However, this is not efficient for real-time planning at the city scale. Similarly, the software SOLCEL (Yoo, 2011) is efficient for evaluating a shading/sunlit area on a solar cell module. However, SOLCEL uses the method from Quaschning and Hanitsch (1998) to calculate the shaded area on a PV module, which requires a survey of the surroundings using optical instruments, such as fish-eye camera. This method is only valid for one observer point (Quaschning and Hanitsch, 1998). Therefore, SOLCEL is not applicable for large PV systems planning like the city scale. The Nguyen and Joshua algorithm (2012) is based on 2.5D raster data, which limits consideration to roofs but not walls or the reflected component of global radiation. However, Redweik et al. (2013) found the solar radiation incident on the walls is lower than that on the roofs, but due to their large collective area, walls are a significant part of the solar-energy potential in urban areas.

1.3. Contribution

In the first part of this paper, we present a 3D SOlar RAdiation Model (SORAM) that builds on the improved Perez et al. (1990) model, the Reindl et al. (1990) model and Sun–Earth trigonometric relationship models from Duffie and Beckman (1980), and also uses a ray-tracing method (Shirley et al., 2005; Mena-Chalco, 2010), which is not subject to the above limitations. SORAM divides the sky into a large number (typically thousands) of uniformly-spaced sectors. This is in contrast with the well-known Perez et al. (1990) model which calculates the contribution of diffuse radiation from three different regions of the sky (horizon band, circum-solar and the rest of the sky), and has previously been shown to perform well in model inter-comparison studies (Muneer, 2004; Noorian et al., 2008). The first modeling novelty is that we combine a ray-tracing method (Shirley et al., 2005; Mena-Chalco, 2010) with the adjusted Perez et al. (1990) model to determine whether a solar ray (direct or diffuse), can reach a PV cell location in the 3D terrain map. The angle of incidence of each solar ray is taken into account since for a sloping surface, each solar ray from the sky contributes different amounts of solar energy.

In SORAM, we also utilize the model developed by Reindl et al. (1990) to split measured values of hourly global radiation into its direct and diffuse components.

The data thus derived are then corrected for the inclined plane of the PV cell by taking into account geometry (i.e. solar altitude, solar azimuth, and azimuth and elevation of the PV cell), as well as the shadows projected by surrounding objects. By aggregating the direct and diffuse radiation from all the points taking into account the angles of incidence in the sky that are not obstructed by obstacles, SORAM can accurately obtain the tilted global radiation received by a sloping PV cell over any period of time, from 1 h to one year. We validate our results both against the well-known Perez et al. (1990) model without terrain obstacles, and against the global radiation measured by the sensors surrounded by real urban obstacles (Sheffield Solar Farm, 2013).

Different from GRASS GIS r.sun and PVSYST, SORAM calculates solar radiation receipt based on an anisotropic sky. Also, unlike Melo et al. (2013) and Redweik et al. (2013), SORAM takes into account the angle of incidence of each sky segment by deducing the solar-energy contribution for each segment separately, based on the Perez et al. (1990) model for the calculation of diffuse radiation.

SORAM also has several ways of enabling greater future scalability than the other software tools and models mentioned above. The first advantage is because the segment of the sky in SORAM is modular. Therefore, in order to increase modeling accuracy of the anisotropic nature of diffuse radiation, SORAM can be easily scaled to incorporate a more sophisticated method and/or increase the spatial resolution of sky segment. The second advantage of SORAM is that because it uses the angle of incidence from the Sun to a point on a PV cell for each solar (direct and diffuse) ray, it can be used to calculate the solar radiation received by various shapes of panel element such as a cylinder (which is already used in the solar PV industry) and is not limited to just a flat plane surface (McIntosh et al., 2007; Colantuono et al., 2013); in other words, various models of solar concentrators can be embedded into SORAM to operate a comprehensive optimization analysis. However, here, for simplification and because it is widely employed in industry, we just use a flat plane surface in our analysis. The third advantage of SORAM is that since a 2-axis PV tracker moves according to the position of the Sun, meaning that the tracker's coordinates are available, SORAM can easily calculate shading losses resulting from other trackers in the PV collector field.

It is also worth noting that in the field of radio-communications (Boithais, 1987), a number of tools have been developed which predict the propagation of electromagnetic waves (Atoll, 2013). Despite the common electromagnetic nature of radio-communication waves and sun rays, there are some fundamental differences when considering propagation:

1. Propagation path: radio waves are emitted from devices on Earth's surface, whereas sun rays come from a single source in the sky and are parallel. Therefore, radio wave propagation deals mainly with how waves reflect and penetrate structures, whereas solar ray propagation is affected by atmospheric effects as well as how rays intersect ground-level obstacles.
2. Frequency: radio wave propagation ($\sim 10^9$ Hz) can be treated as a wave model, whereas visible solar ray propagation ($\sim 10^{15}$ Hz) is treated as a ray model.

Therefore, the contribution of this paper overlaps to a certain extent with radio-wave propagation research, but is fundamentally different in the aforementioned areas. The common aspects may be important for radio-wave flux estimates in an urban environment.

2. The 3D urban environment

This section describes the 3D urban environment used to demonstrate our proposed methodology. The solar position data in terms of hourly solar altitude, solar azimuth, angle of incidence on a PV cell's surface, and daily solar duration are computed by SORAM based on models found in Duffie and Beckman (1980). Fig. 1 outlines the overall structure of the model flowchart that underpins this body of work. In this figure, the solar altitude, solar azimuth, solar duration and angle of incidence are derived using the solar geometry algorithm summarized in Fig. 2. The parameters marked as "daily" are daily values, otherwise they are hourly values. All parameters are calculated at an hourly temporal resolution.

2.1. Direct and diffuse radiation

For each day, the sunrise time is determined and solar radiation data from that point onwards are integrated until sunset. This is to avoid unnecessary calculations for the night-time hours, to save computation time. Horizontal direct and diffuse radiation data are required to estimate global radiation on a PV cell of a given slope and azimuth. Global solar radiation received by a PV cell can be decomposed into direct and diffuse components. Although horizontal global radiation data are commonly available, horizontal direct and diffuse radiation are scarcely measured variables because of costs; therefore, the widely used model developed by Reindl et al. (1990) is embedded into SORAM to predict hourly direct and diffuse radiation from hourly global radiation on a horizontal PV cell.

Sections 3 and 4 outline the algorithm that estimates direct and diffuse radiation on a PV cell of given slope and azimuth from their counterparts on a horizontal PV cell considering surrounding shading conditions. In SORAM, for visualization and demonstration, a PV cell can be represented by an arbitrary area, which is taken to be a triangle in this particular paper. As shown in Fig. 3, the plan and portrait view of a PV cell are represented by a triangle in a hypothetical city in SORAM. The red dots on the PV cell represent the diffuse rays with

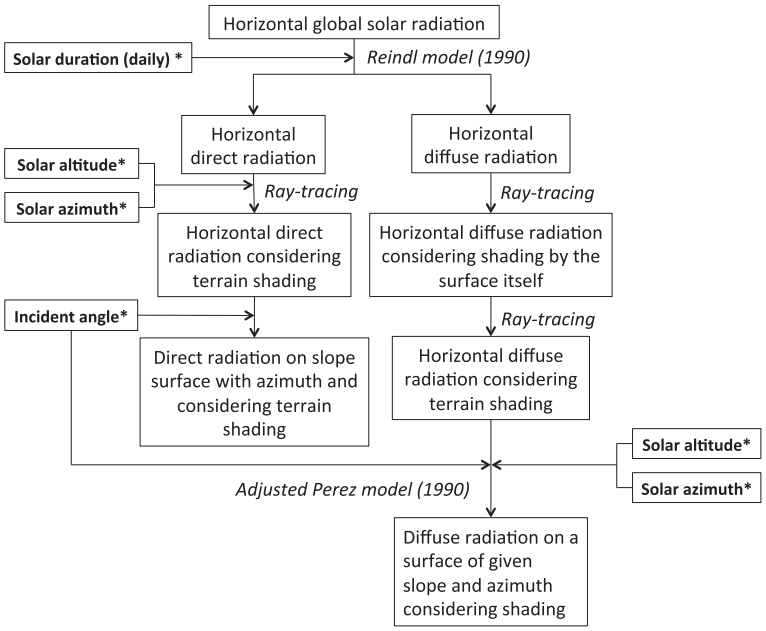

Fig. 1. Flowchart of SORAM. Solar altitude, solar azimuth, solar duration and angle of incidence are derived from the process summarized in Fig. 2. The parameters marked as "daily" are daily values, otherwise hourly values.

their angles of incidence smaller than 0° or greater than 90°.

The angle of incidence of each solar ray is calculated using a solar geometry sub-function, and the resulting flowchart is shown in Fig. 2. The angle of incidence at a given time is assumed constant for the whole map area. The parameters defining the position of the Sun in the sky are calculated on a daily or hourly basis; a list of them can be found in Table 1. For more details, see Duffie and Beckman (1980).

2.2. Shading algorithm

In order to simulate a random urban setting, a number of obstacles (buildings/trees) are incorporated with stochastic width, length and height dimensions, with boundaries of [1, 10], [1, 10] and [1, 50] m respectively (i.e. these values are randomly varied in 1-m increments within these ranges). The aim of using these boundaries is to obtain a realistic representation of the city and solar radiation distribution for visualization. When we incorporate a real urban plan into SORAM, these hypothetical boundaries are no longer necessary. In this work, trees are considered as solid obstacles and their solar energy potential is not considered. The dimension for each building/tree is described by using its two-set cartesian coordinates in this 3D environment, i.e. (x, y, z) and $(x + \text{width}, y + \text{length}, z + \text{height})$. These random obstacles are also randomly placed on a $100 \times 100\ m^2$ map showing their distribution. Results are sampled at a 1×1 m spatial resolution on this map. Solar altitude varies between [0°, 90°], and the solar azimuth angle ranges between −180° and 180° with 0° due south, where east is negative and west is positive. The time-step size depends on the resolution at which solar radiation is observed. Hourly temporal resolution is sufficient for most applications (Hofierka and Zlocha, 2012), and is consequently adopted in this work.

Ray-tracing (Shirley et al., 2005; Mena-Chalco, 2010) is used in this work to determine if a solar ray is shaded by an obstacle. Shirley et al. (2005) considered an intersection between a 2D ray vector and a rectangle, which can be generalized to between a arbitrary 3D ray and a voxel. Mena-Chalco (2010) implemented the ray-tracing algorithm for detecting if a 3D ray vector intersects with a box (voxel). In our ray-tracing algorithm, contrary to real

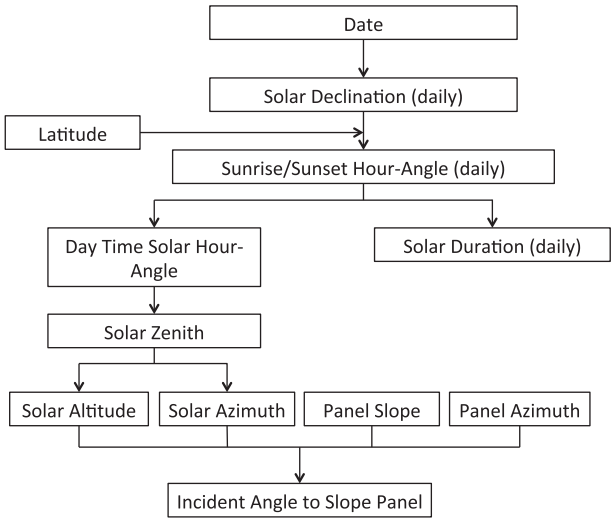

Fig. 2. Flowchart of the solar geometry calculation used to derive solar altitude, solar azimuth, solar duration and angle of incidence. The parameters marked as "daily" are daily values, otherwise hourly values.

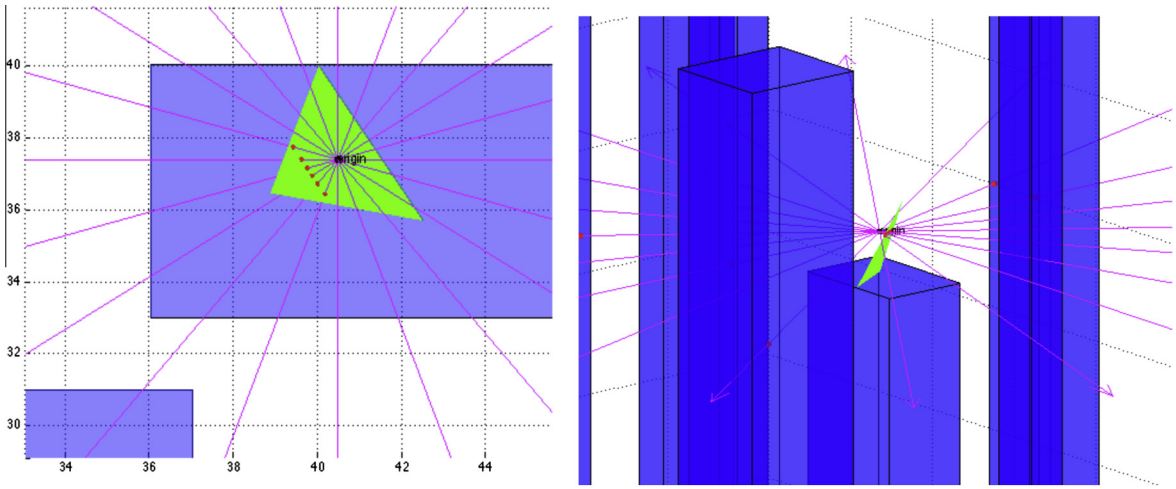

Fig. 3. The red dots on the PV cell represent the diffuse rays with $\theta_d \leqslant 0^\circ$ or $\theta_d \geqslant 90^\circ$. (a) Plan view of a PV cell represented by a triangle in a hypothetical city in SORAM; (b) portrait view of (a). (For interpretation of the references to colour in this figure legend, the reader is referred to the web version of this article.)

Table 1
Nomenclature used in this paper.

Parameter name	Parameter	Range
Angle of incidence from direct radiation	θ	0–90°
Angle of incidence from diffuse radiation	θ_d	0–90°
Solar altitude	α_s	0–90°
Solar azimuth	γ_s	−180° to 180°
Diffuse-ray altitude	α_d	0–90°
Diffuse-ray azimuth	γ_d	−180° to 180°
Surface slope angle	s	0–90°
Surface azimuth angle	γ	−180° to 180°
Horizontal direct radiation	B_h	0–∞
Slope direct radiation	B_s	0–∞
Horizontal diffuse radiation	D_h	0–∞
Slope diffuse radiation	D_s	0–∞
Diffuse radiation (main)	T_m	0–∞
Diffuse radiation (horizon)	T_h	0–∞
Number of solar ray (main)	n_m	0–∞
Number of solar ray (horizon)	n_h	0–∞
Diffuse radiation contribution coefficient (main)	1	1
Diffuse radiation contribution coefficient (circum-solar)	F_1	0–∞
Diffuse radiation contribution coefficient (horizon)	F_2	0–∞

conditions, a PV cell (i.e. a tested point in the 3D urban environment) is regarded as a source emitting rays to the sky segments. The position of the 3D ray vector on the 3D urban environment is determined by the cartesian coordinates of the tested point; the direction of the 3D ray vector is represented by the hourly altitude (α) and azimuth (γ) of direct/diffuse radiation rays, i.e. $(\sin(\gamma_s), \cos(\gamma_s), \tan(\alpha_s))$ or $(\sin(\gamma_d), \cos(\gamma_d), \tan(\alpha_d))$. The subscripts s means direct solar radiation, and d means diffuse solar radiation. The ray-tracing method is then used between the 3D ray vector and each obstacle. Once a intersection is detected, the distance between the PV cell and the intersection is calculated. A positive distance means the intersection is between the PV cell and the sky, otherwise a negative distance represents an invalid intersection and is discarded.

3. Direct radiation

To predict the tilted direct radiation, a point for mounting a PV panel in SORAM is chosen, called the *origin*. Hourly direct radiation is treated as a ray emanating from the Sun towards of the *origin*. θ is the angle of incidence, i.e. the angle between the direct radiation on a PV cell surface and the normal to that surface.

If $\theta < 0^\circ$ or $\theta \geqslant 90^\circ$, hourly amount of direct radiation associated with the solar ray is excluded from the integration, i.e. $B_s = 0$. Whereas, if $0^\circ \leqslant \theta < 90^\circ$, the ray-tracing algorithm is used to determine whether the direct ray intersects with buildings that are taller than the vertical height of the *origin*. If there is an intersection, $B_s = 0$; if the direct ray is not obstructed by any building, the tilted hourly direct radiation can be estimated by:

$$\begin{aligned} B_s &= B_h \frac{a_0}{a_1}, \\ a_0 &= \max(0, \cos(\theta)), \\ a_1 &= \max\left(\cos(85^\circ), \cos\left(\frac{\pi}{2} - \alpha_s\right)\right). \end{aligned} \tag{1}$$

where B_s and B_h are the hourly direct radiation on a sloping and horizontal PV cell, respectively, α_s is the solar altitude angle. For more details of these variables, see Duffie and Beckman (1980).

4. Diffuse radiation

In this section, we describe how SORAM converts diffuse radiation from horizontal surface to the sloping one while taking shading into account. As previously mentioned, the Perez et al. (1990) model has demonstrated strong agreement with empirical data. In SORAM, the Perez et al. (1990) model is further developed to take shading due to obstacles into account.

4.1. Augmenting Perez et al. model with ray-tracing

It is observed that, in the atmosphere, there are two main zones causing the anisotropic nature of diffuse radiation: (i) circumsolar brightening resulting from forward scattering by aerosols, and (ii) horizon brightening mostly caused by multiple Rayleigh scattering and retro-scattering in a clear atmosphere (Kano, 1964). In the Perez et al. (1990) model, the circumsolar disk and horizon band are superimposed on the sky hemisphere, creating three distinct isotropic zones (Perez et al., 1987).

In the model proposed by Perez et al. (1990), for simplicity it is assumed that all circumsolar energy is emitted from a point centred on the Sun's position, and the horizon band originates from an arc of a great circle at the base of the atmosphere. The horizon band in SORAM is a great circle that is at the same height as the *origin*, and because it is naturally level with the *origin*, it has no effect on a horizontal PV cell centred on the *origin*.

Without any terrain shading, the relationship between diffuse radiation on a sloping PV cell and a horizontal one may be written as (Perez et al., 1987, 1990):

$$D_s = D_h\left[(1-F_1)\frac{1+\cos(s)}{2} + F_1\frac{a_0}{a_1} + F_2\sin(s)\right]. \tag{2}$$

where D_s and D_h are the hourly diffuse radiation on a sloping and horizontal PV cell, respectively, a_0 and a_1 have the same definition as in Eqs. 1, s is the slope angle of a PV cell, F_1 and F_2 are the diffuse radiation contribution coefficients for the circumsolar and horizon zones, respectively. They are normalised by the diffuse radiation contribution coefficient for the main zone. Therefore, $(1-F_1)$ is the ratio of diffuse radiation on a horizontal PV cell from the main zone to the whole sky.

Because of the homogeneity of the three aforementioned sky zones, applying the Perez et al. (1990) model to SORAM and assuming the total diffuse radiation from the main zone is T_m, the number of those diffuse rays is n_m, we note that:

$$1-F_1 = \int_{-\pi}^{\pi}\int_0^{\frac{\pi}{2}}\frac{T_m}{n_m}\sin(\alpha_d)\,d\alpha_d d\gamma_d, \tag{3}$$

where α_d and γ_d are the altitude and azimuth angles for each diffuse ray, respectively. Thus, the diffuse radiation contribution of each ray in the sky is,

$$\frac{T_m}{n_m} = \frac{1-F_1}{\int_{-\pi}^{\pi}\int_0^{\frac{\pi}{2}}\sin(\alpha_d)\,d\alpha_d d\gamma_d}, = \frac{1-F_1}{2\pi}, \tag{4}$$

Moreover, the angle of incidence of a diffuse ray is

$$\cos(\theta_d) = \cos\left(\frac{\pi}{2}-\alpha_d\right)\cos(s), + \sin\left(\frac{\pi}{2}-\alpha_d\right)\sin(s)\cos(\gamma_d-\gamma), \tag{5}$$

where γ is the azimuth angle of a PV cell.

Therefore, without any terrain shading, the diffuse radiation from the main zone both on the front and back of a sloping PV cell is,

$$\int\frac{T_m}{n_m}\cos(\theta_d)\,d\theta_d, = \frac{1-F_1}{2\pi}\cos(s)\int_{-\pi}^{\pi}\int_0^{\frac{\pi}{2}}\sin(\alpha_d)\,d\alpha_d d\gamma_d, = (1-F_1)\cos(s). \tag{6}$$

This part of the diffuse radiation contribution is for the whole main zone of the sky. This means when a diffuse ray comes from back of a PV cell ($\theta < 0^\circ$ or $\theta > 90^\circ$), a negative value contributes to this integration, which should be zero. Thus, the diffuse radiation contribution shaded by a PV cell needs to be added, which is,

$$(1-F_1)\frac{1-\cos(s)}{2}. \tag{7}$$

Therefore in reality, when there is no terrain shading, the diffuse radiation from the main zone on a sloping PV cell is,

$$(1-F_1)\cos(s) + (1-F_1)\frac{1-\cos(s)}{2}, = (1-F_1)\frac{\cos(s)+1}{2}. \tag{8}$$

which satisfies Perez et al. (1987),Perez et al. (1990) as shown in Eq. 2. Note that in SORAM, the part of diffuse radiation contribution comes from back of a PV cell is detected and set to be zero.

Similar to the direct radiation, the conversion of horizontal to inclined diffuse radiation from the circumsolar zone is,

$$F_1\frac{a_0}{a_1}. \tag{9}$$

Assuming the total diffuse radiation from the horizon zone is T_h and the number of those diffuse rays is n_h, we have:

$$F_2\sin(s) = \int\frac{T_h}{n_h}\cos(\theta_d)\,d\theta_d, = \frac{T_m}{n_m}\int_{\gamma-\frac{\pi}{2}}^{\gamma+\frac{\pi}{2}}\sin(s)\cos(\gamma_d-\gamma)\,d\gamma_d, \tag{10}$$

Thus,

$$\frac{T_h}{n_h} = \frac{F_2}{\int_{\gamma-\frac{\pi}{2}}^{\gamma+\frac{\pi}{2}} \cos(\gamma_d - \gamma)\, d\gamma_d}. \tag{11}$$

To sum up, for each diffuse ray in the main, circumsolar and horizon zone, the energy contributions are

$$\frac{1 - F_1}{\int_{-\pi}^{\pi} \int_0^{\frac{\pi}{2}} \sin(\alpha_d)\, d\alpha_d d\gamma_d} \cos(\theta_d), \tag{12}$$

$$F_1 \frac{a_0}{a_1}, \tag{13}$$

$$\frac{F_2}{\int_{\gamma-\frac{\pi}{2}}^{\gamma+\frac{\pi}{2}} \cos(\gamma_d - \gamma)\, d\gamma_d}. \cos(\theta_d). \tag{14}$$

4.2. Shading from slope surface and terrain

Figs. 3 and 4 show an arbitrary example where the triangle represents a PV cell with a slope of 50° and an azimuth angle 60° southwest facing in SORAM. A half sphere with altitude $\alpha_d \in [0°, 90°]$ and azimuth $\gamma_d \in [-180°, 180°]$, respectively, is centred on the *origin*. Vectors in Fig. 3 and 4 represent twenty diffuse rays ($\alpha_d = 0°$).

Let the number of vectors when $\alpha_d = 0°$ be N. To guarantee the uniform representation of the sky, the number of vectors for any elevation should be $N\cos(\alpha_d)$. It is worth noting that as the slope angle increases, the number of independent vectors converges to one.

There are two kinds of shading: one results from the sloping PV cell itself, and the other is from surrounding obstacles including buildings. If $\theta_d < 0°$ or $\theta_d \geqslant 90°, D_s = 0$. Whereas, if $0° \leqslant \theta_d < 90°$, ray-tracing algorithm is used to determine whether or not the diffuse ray intersects with buildings. If there is an intersection, $D_s = 0$; otherwise, if a diffuse ray emanates from the main, the circumsolar or the horizon zone, this ray's energy is given by Eqs. 12,13 or 14, respectively, and is therefore integrated to the diffuse portion, see Fig. 4.

Finally, when all diffuse rays are aggregated, the diffuse portion is multiplied by the hourly observed horizontal diffuse radiation to obtain the tilted diffuse radiation. This is then added to the direct radiation calculated from Section 3 at the same time-step to obtain the tilted global radiation.

5. Results and evaluation

5.1. Hypothetic results

Integrating results from the above calculations for a certain time period for each point on the map, a contour plot is constructed, as shown in Fig. 5. Fig. 5a shows stacked contours for a sequence of height levels spaced by 20 m, in each case considering shading from the hypothetical distribution of buildings. Next, Fig. 5b with its chosable parameters (height, slope and azimuth) displays the solar radiation distribution on the ground due to shading with its chosable parameters.

SORAM can also deduce the optimised slope and azimuth angle for any selected location in a city. This is accomplished by repeatedly running SORAM for a given range of slope and azimuth angles.

5.2. Evaluation of SORAM

The Sheffield Solar Farm (SSF) is part of Project Sunshine operating at the University of Sheffield, UK, allowing real-world testing of photovoltaics. Nine months of hourly global radiation data were collected by the SSF with two different pyranometers at a 12.7° tilt, 45° southeast facing and 45° southwest facing, respectively. Fig. 6a shows a Google Maps image of the Hicks Building at the University of Sheffield, UK and the resulting map in SORAM. The green triangle represents the position of the pyranometer from the Sheffield Solar Farm. Fig. 6b and c show a graphical sketch of how SORAM takes obstacles into account when determining the amount of diffuse radiation reaching the pyranometer. The blue lines represent the edges of surrounding buildings that can cast shadows on the green triangle representing the pyranometer position. The magenta vectors in Fig. 6b and c indicate the part of diffuse radiation when the slope angle of the pyranometer (green triangle) is 12.7°, and the actual stepsize of azimuth used in SORAM is one-tenth or smaller than shown in this figure. Fig. 7 shows the global radiation distribution over the sampled area around Hicks building. The blue lines in Fig. 7a and b depict the edges of buildings of the sampled area based on a Google Map and SORAM. All the obstacles such as buildings and trees are approximated by voxels. Fig. 7c displays the 3D simulation of global radiation distribution at heights of 0 m and 11.3 m over area defined in Fig. 7a and b, based on SORAM and accounting for the various buildings present.

The performance output of SORAM is shown in Tables 2 and 3. The evaluation includes the mean bias error (MBE), given by

$$\mathrm{MBE} = \frac{\sum_n (\mathrm{model}_i - \mathrm{measured}_i)}{n}, \tag{15}$$

where n is the number of data points and i denotes a given event, and root mean square error (RMSE),

$$\mathrm{RMSE} = \left\{ \frac{\sum_n (\mathrm{model}_i - \mathrm{measured}_i)^2}{n} \right\}^{0.5}. \tag{16}$$

Experiments about the step sizes of α_d and γ_d have been done in SORAM, i.e. resolution of the segment of the diffuse radiation from the sky. The differences of MBE and RMSE between experiments should be smaller than 1%, because 1% increase/decrease is very important in PV industry. Without any terrain shading, the MBE and RMSE are calculated in the way that SORAM produces the modelled data, and the output from Perez et al.

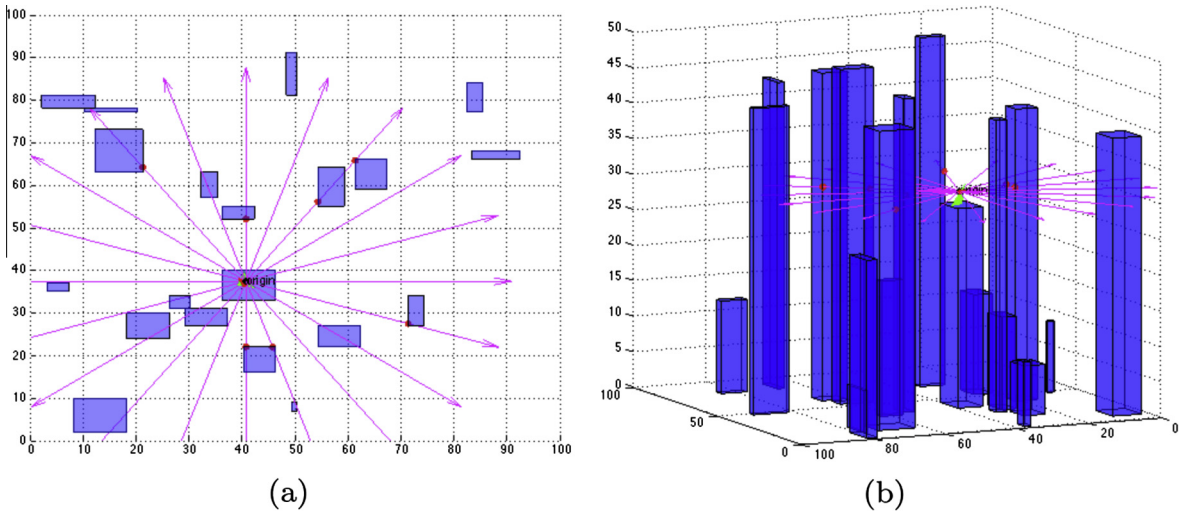

Fig. 4. The red dots on buildings mean the diffuse ray intersect a building and are therefore not collected by the PV cell; while the red dots on the PV cell represent the diffuse rays with $\theta_d \leqslant 0^\circ$ or $\theta_d \geqslant 90^\circ$. (a) Plan view of a hypothetical city in SORAM; (b) portrait view. (For interpretation of the references to colour in this figure legend, the reader is referred to the web version of this article.)

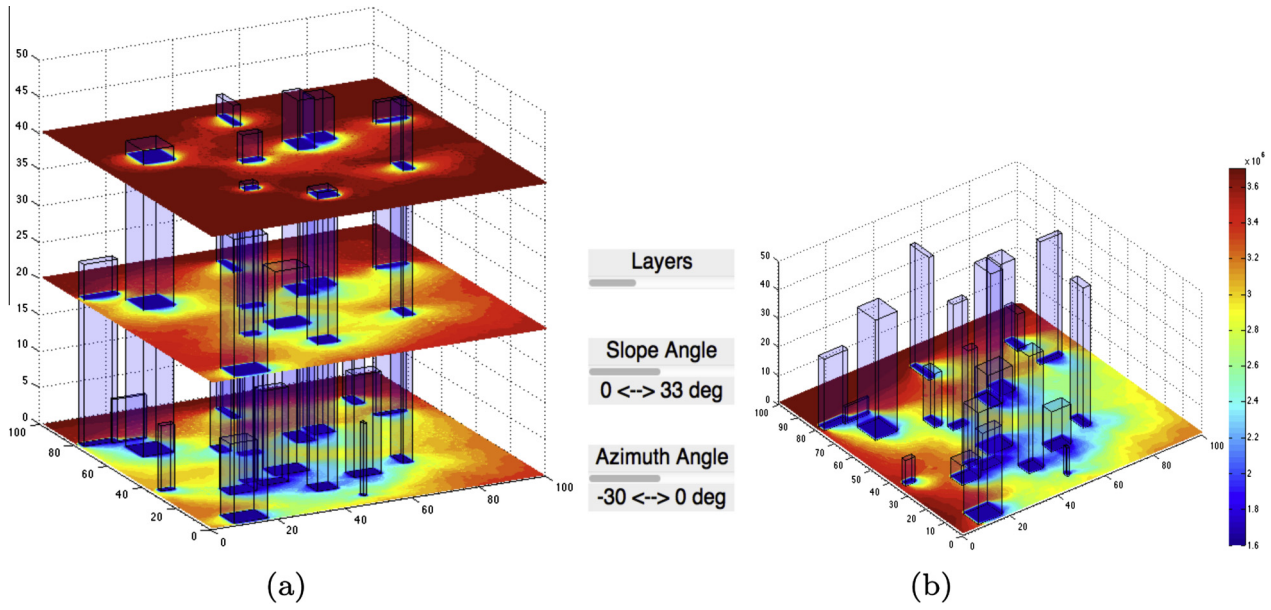

Fig. 5. Solar radiation distribution in the hypothetical city introduced in Fig. 4 computed by SORAM: (a) contours on various heights; and (b) contours with chosable parameters: height, slope and azimuth angles of PV cells.

(1990) model is treated as the measured data. In this case, the maximum step size of α_d and γ_d is 6°. Under terrain shading, SORAM with various step sizes produces the modelled data, and SSF gives the measured data. In this case, the maximum step size of α_d and γ_d is 2°. These experiments were done with 1° increment, and start from 1° for the step sizes of α_d and γ_d due to computer limitation and time.

In Table 2, SORAM outputs the modelled data, and the data from the Perez et al. (1990) model is treated as the measured data. The performance is evaluated using the ratio of sloping diffuse radiation to horizontal diffuse radiation: this step is to check if the improved diffuse model in SORAM matches the Perez et al. (1990) model. This table shows a $-3.6 \times 10^{-3}\%$ underestimation of SORAM against the Perez et al. (1990) model, and the RMSE is $3.4 \times 10^{-2}\%$. In order to evaluate how consistent SORAM is with the Perez et al. (1990) model, the step size of α_d and γ_d of 1° is used. These results indicate that the formulae deduced in Section 4 are consistent with the Perez et al. (1990) model.

Similarly, Table 3 shows the comparison between SORAM and the observed SSF data, and, between the Perez et al. (1990) model and the observed SSF data. The performance is evaluated using the global irradiance since this step is to validate SORAM. The "SORAM" shown

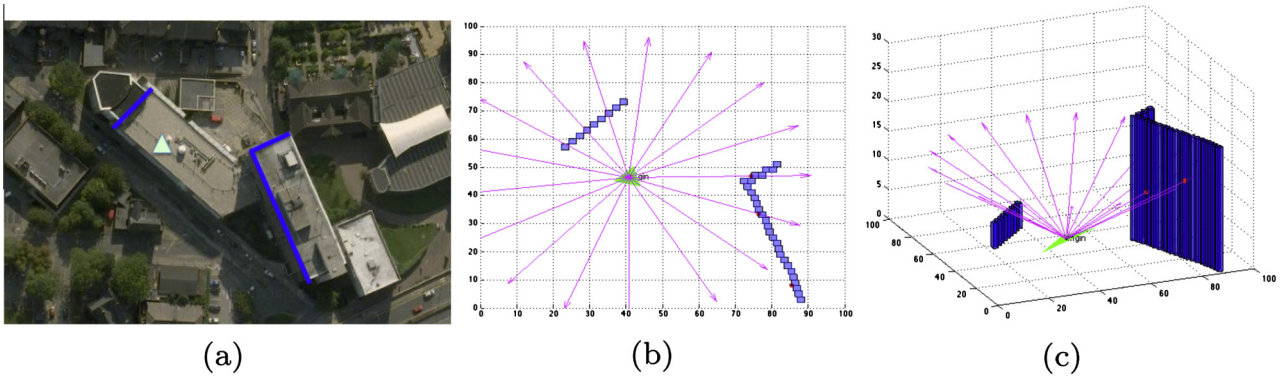

Fig. 6. (a) GoogleMap's image of the Hicks Building at the University of Sheffield, UK; the green triangle represents a PV cell (i.e. the position of the pyranometer from the Sheffield Solar Farm); (b), (c) A graphical sketch of how SORAM takes obstacles into account when determining the amount of diffuse radiation reaching the PV cell. (For interpretation of the references to colour in this figure legend, the reader is referred to the web version of this article.)

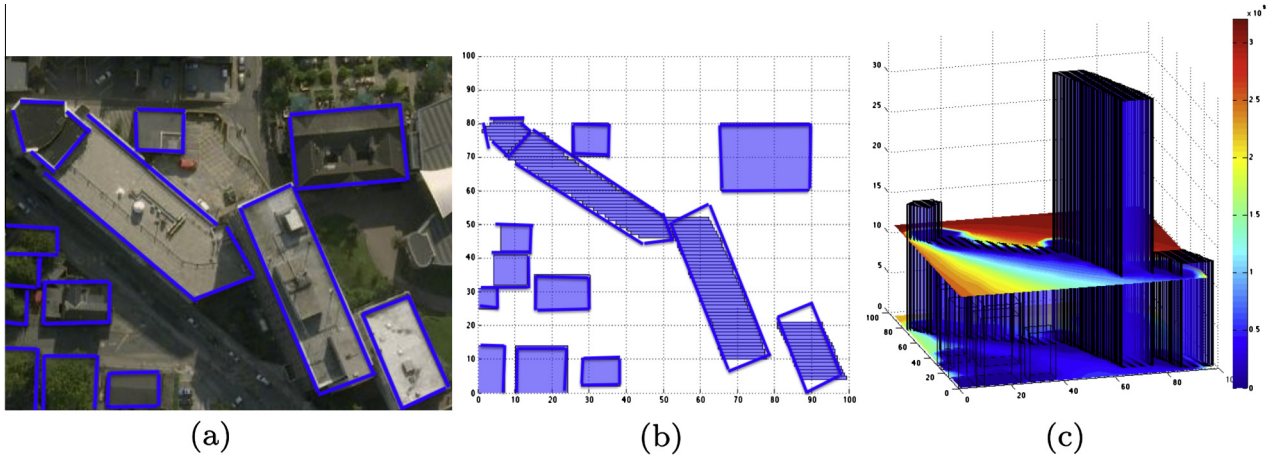

Fig. 7. (a) GoogleMap image of Hicks Building and its immediate surroundings at the University of Sheffield, UK; (b) plan view of (a); (c) 3D simulation of global radiation distribution at heights of 0 m and 11.3 m over area defined in (a) and (b), based on SORAM described in main text and accounting for the various buildings present. The blue lines in (a) and (b) depict the margins of buildings of the sampled area both from a Google Map and SORAM. All the obstacles such as buildings and trees are approximated by voxels. (For interpretation of the references to color in this figure legend, the reader is referred to the web version of this article.)

Table 2
Output performance of SORAM vs the Perez et al. (1990) model. The output is the ratio of diffuse radiation on a sloping PV cell to a horizontal one. The minus sign in MBE means the output from SORAM underestimates that from the Perez et al. (1990) model.

Orientation	Mean	MBE	RMSE
45° SE	1.1	-2.8×10^{-5}	1.9×10^{-4}
45° SW	1.0	-4.9×10^{-5}	5.3×10^{-4}
Percent error		-3.6×10^{-3}%	3.4×10^{-2} %

Table 3
Output performance of SORAM and Perez et al. models (1990) vs observed data from the Sheffield Solar Farm. The unit of mean global irradiance, MBE and RMSE is KJ m^{-2} h^{-1}. The minus sign in MBE of SORAM means the output from SORAM underestimates that from the Sheffield Solar Farm measured global radiation data.

Surface	Mean global	SORAM		Perez et al. model	
Orientation	Irradiance	MBE	RMSE	MBE	RMSE
45° SE	912.1	45.8	177.2	72.6	196.5
45° SW	794.0	−13.2	121.5	9.6	103.5
Percent error		3.3%	17.4%	4.6%	17.3%

in Table 3 depicts that SORAM ran under real shading conditions around the *origin*. In this case, SORAM gives the modelled data, and SSF gives the measured data. The shading is mainly caused by two parts of Hicks building with absolute heights (higher than the *origin*) of 21.9 m and 4.3 m respectively, as shown in Fig. 6. Note that the Perez et al. (1990) model is not able to integrate the shading effect from the surroundings. Therefore the diffuse radiation produced by SORAM is smaller than the Perez et al. (1990) model due to shading (Table 3). Considering computation time, the step size of α_d and γ_d is 2° for this table.

Furthermore, SSF's horizontal global radiation has been measured under the same shading conditions (the green triangle in Fig. 6 shows the position of the SSF's

pyranometers), and used to predict the tilted direct and diffuse radiation for the tilt-orientated PV cell. However, in order to calculate solar radiation on a shaded sloping PV cell, SORAM input should be unshaded horizontal global radiation, which is not available in Sheffield. Therefore, we expected that SORAM modelled output would underestimate the solar energy. The evaluation, between the 45° SW pyranometer from SSF and SORAM modelled output under the same configuration and shadow effects as shown in SORAM in Table 3, meets the expectation whose MBE is -13.2 KJ m^{-2} h^{-1}; however, for the 45° SE case, it does not. There are at least three reasons for these errors, regardless of the overestimation or underestimation. The first reason is the complexity of the 45° SE surroundings, where only the Hicks building (main shadow) is taken into account, whereas several buildings of unknown heights that could cast shadows on the pyranometer are not included in SORAM. Secondly, the modelled solar radiation is sensitive to the positions of the pyranometer (the triangle in Fig. 6b and c) and the buildings, while the real-life map in SORAM (Fig. 6b and c) is just an approximation constructed from Google Map: thus this approximation may produce errors. Thirdly, it is believed that the largest errors are introduced by the embedded Perez et al. (1990) model, which treats the solar radiation contribution within each sky zone as uniform, and from errors in the solar-radiation measurements.

The absolute averaged MBE of SORAM with shading against the observed data is 3.3% while RMSE is 17.4%: MBE (RMSE) is smaller than (similar to) the MBE (RMSE) of 4.6% (17.3%) obtained using the Perez et al. (1990) model against measured data. Overall, SORAM shows a better and more accurate performance than the Perez et al. (1990) model.

6. Conclusion

In this paper, we propose a numerical model (SORAM) for evaluating the direct and diffuse solar radiation on a sloping PV cell in an urban environment. We believe this is a key enabler technology with great potential for the mass deployment of solar PV cells in current and future sustainable cities.

The paper makes three key contributions. First, the established Perez et al. (1990) model is combined with a ray-tracing algorithm to improve the accuracy of anisotropic diffuse radiation modeling, taking into account the angle of incidence of each solar ray. Second, dynamic 3D shading from urban obstacles (buildings/trees) is integrated into the model. Third, the model is validated using empirical measurement.

More specifically, the paper utilizes the Reindl et al. model (1990) to convert global horizontal radiation to direct and diffuse radiation. The direct radiation on a PV cell of a given slope and azimuth is determined following Duffie and Beckman (1980) and Muneer (2004), together with a ray-tracing algorithm. The Perez et al. (1990) model is adapted with a ray-tracing algorithm, in order to transform diffuse radiation from a patch in the sky to a specific ray. The combined algorithm is then used to compute the shading effect from the urban terrain buildings. Finally, we aggregate the direct and diffuse radiation received.

SORAM without shading is validated against the Perez et al. (1990) model. A -3.6×10^{-3}% underestimation show that under conditions of no shading SORAM works as well as the Perez et al. (1990) model. SORAM with shading is evaluated against the observed SSF solar radiation data. The results show a 3.3% MBE and a 17.4% RMSE, while these values are respectively 4.6% and 17.3% when the outputs from the Perez et al. (1990) model are compared with SSF data. Therefore, SORAM overall performs better than the Perez et al. (1990) model.

The proposed model has been applied to a sample area in order to demonstrate its capabilities. Error analysis shows that SORAM can be effectively used in many applications including solar energy (PV and thermal) installations and environmentally friendly urban design. A further development of SORAM will focus on flexibility of shapes of obstacles and integrating reflected radiation by different materials such as glass and trees.

For queries about the SORAM computer code, please contact the corresponding author. For queries about the experimental data used here, please contact Dr. Alastair Buckley (alastair.buckley@sheffield.ac.uk) from the Sheffield Solar Farm (www.sheffieldsolarfarm.group.shef.ac.uk) who is the PI of SSF.

Acknowledgements

This work was partially conducted on measurements taken by the Sheffield Solar Farm,Sheffield Solar Farm (2013). We would like to thank Google Map. RE acknowledges M. Keray for patient encouragement and is also grateful to NSF, Hungary (OTKA, Ref. No. K83133) for financial support received.

References

ArcGIS Help 10.1., 2012. [Internet]. http://resources.arcgis.com/en/help/main/10.1/index.html#/Understanding_solar_radiation_analysis/009z000000t8000000/.

Atoll, F., 2013. http://www.forsk.com/atoll/.

Boithais, L., 1987. Radio Wave Propagation. McGraw-Hill Book Company, New York.

Colantuono, G., Buckley, A., Erdelyi, R., 2013. Ray-optics modelling of rectangular and cylindrical 2-layer solar concentrators. J. Lightw. Technol. 31 (7), 1033–1044.

da Silva Jardim, C., Rther, R., Salamoni, I.T., de Souza Viana, T., Rebechi, S.H., Knob, P.J., 2008. The strategic siting and the roofing area requirements of building-integrated photovoltaic solar energy generators in urban areas in Brazil. Energy Build. 40, 365–370.

Duffie, J.A., Beckman, W.A., 1980. Solar Engineering of Thermal Processes. John Wiley & Sons, Inc., pp.13–45.

Fartaria, T.O., Pereira, M.C., 2013. Simulation and computation of shadow losses of direct normal, diffuse solar radiation and albedo in a photovoltaic field with multiple 2-axis trackers using ray tracing methods. Solar Energy 91, 93–101.

HEMI, 2000. The Solar Analyst 1.0 User Manual Draft. Helios Environmental Modeling Institute 568 (HEMI), LLC. Kansas, KS.
Hofierka, J., Kanuk, J., 2009. Assessment of photovoltaic potential in urban areas using opensource solar radiation tools. Renew. Energy 34, 2206–2214.
Hofierka, J., Zlocha, M., 2012. A new 3-D solar radiation model for 3-D city models. Trans. GIS, 2012 16 (5), 681–690.
Kano, M., 1964. Effect of a Turbid Layer on Radiation Emerging from a Planetary Atmosphere. In: Doctoral Dssertation. University of California, Los Angeles.
Lorenzo, E., Navarte, L., Munoz, J., 2011. Tracking and back-tracking. Prog. Photovolt.: Res. Appl. 19, 747–753.
Melo, E.G., Almeida, M.P., Zilles, R., Grimoni, J.A.B., 2013. Using a shading matrix to estimate the shading factor and the irradiation in a three-dimensional model of a receiving surface in an urban environment. Solar Energy 92, 15–25.
Mena-Chalco, J.P., 2010. Ray/box Intersection. http://www.mathworks.co.uk/matlabcentral/fileexchange/26834-raybox-intersection.
Muneer, T., 2004. Solar radiation and daylight models. Elsevier Butterworth-Heinemann, pp. 165..
McIntosh, K., Yamada, N., Richards, B., 2007. Theoretical comparison of cylindrical and square-planar luminescent solar concentrators. Appl. Phys. B 88, 285–290.
Navarte, L., Lorenzo, E., 2008. Tracking and ground cover ratio. Prog. Photovolt.: Res. Appl. 16, 703–714.
Noorian, A.M., Moradi, I., Kamali, G.A., 2008. Evaluation of 12 models to estimate hourly diffused irradiation on inclined surfaces. Renew. Energy 33, 1406–1412.
Orioli, A., Gangi, A.D., 2012. An improved photographic method to estimate the shading effect of obstructions. Solar Energy 86, 3470–3488.
Perez, R., Ineichen, P., Stewart, R., Menicucci, D., 1987. A new simplified version of the Perez diffuse irradiance model for tilted surfaces. Solar Energy 39 (3), 221–231.
Perez, R., Ineichen, P., Seals, R., Michalsky, J., Stewart, R., 1990. Modeling daylight availability and irradiance components from direct and global irradiance. Solar Energy 44 (5), 271–289.
Perpinan, O., 2012. Cost of energy and mutual shadow in a 2-axis tracking PV system. Renew. Energy 43, 331–342.
PV*Sol, 2013. http://www.solardesign.co.uk/pv.php.
PVSYST, 2013. PVsyst 6 Help. http://files.pvsyst.com/help/index.html.
Quaschning, V., Hanitsch, R., 1998. Irradiance calculation on shaded surfaces. Solar Energy 62 (5), 365–375.
Redweik, P., Catita, C., Brito, M., 2013. Solar energy potential on roofs and facades in an urban landscape. Solar Energy 97, 332–341.
Reindl, D.T., Beckman, W.A., Duffie, J.A., 1990. Diffuse fraction correlations. Solar Energy 45 (1), 1–7.
Sheffield Solar Farm, 2013. http://www.sheffieldsolarfarm.group.shef.ac.uk.
Shirley, P., Gleicher, M., Marschner, S.R., Reinhard, E., Sung, K., Thompson, W.B., Willemsen, P., 2005. Fundamentals of Computer Graphics. A K Peters, Ltd., pp. 218–228.
Suri, M., Hofierka, J., 2004. A new GIS-based solar radiation model and its application to photovoltaic assessments. Trans. GIS 8 (2), 175–190.
Yoo, S.H., 2011. Simulation for an optimal application of BIPV through parameter variation. Solar Energy 85, 1291–1301.